Chemical Engineering Journal 422 (2021) 130091

Contents lists available at ScienceDirect

Chemical Engineering Journal

journal homepage: www.elsevier.com/locate/cej

Silk-based pressure/temperature sensing bimodal ionotronic skin with stimulus discriminability and low temperature workability

Qianying Chen [a,1], Hao Tang [b,1], Jialin Liu [a], Ranran Wang [b], Jing Sun [b], Jinrong Yao [a], Zhengzhong Shao [a], Xin Chen [a,*]

[a] State Key Laboratory of Molecular Engineering of Polymers, Department of Macromolecular Science, Shanghai Stomatological Hospital, Laboratory of Advanced Materials, Fudan University, 220 Handan Road, Shanghai 200433, People's Republic of China

[b] State Key Laboratory of High Performance Ceramics and Superfine Microstructure, Shanghai Institute of Ceramics, Chinese Academy of Sciences, 585 Heshuo Road, Shanghai 201899, People's Republic of China

ARTICLE INFO

Keywords:
Silk protein
Hydrogels
Ionotronic skin
Environmental sensitivity
Dual responsibility

ABSTRACT

Multi-responsive sensing devices have contributed extensively to health monitoring applications. However, the effects of different stimuli often confuse, and thus cause, signal distortion of the sensor response. In addition, many sensing devices cannot work properly at low temperatures. In the present study, a robust regenerated silk fibroin (RSF)-based hydrogel was fabricated with silver nanowires (AgNWs) embedded in the surface. The microstructure of AgNW-embedded RSF surface was introduced using cotton fabric as a template. Afterwards, the hydrogel was immersed in an aqueous calcium chloride solution to introduce Ca(II) ions into the matrix of the RSF hydrogel. Finally, two pieces of the RSF/AgNW/Ca(II) hydrogel were assembled with AgNW layer face-to-face to form a dual-responsive ionotronic skin that was sensitive to pressure and temperature. The pressure-response of the RSF/AgNW/Ca(II) ionotronic skin showed a high sensitivity, short response time, and good durability. In addition, the temperature-response also showed a high sensitivity and good durability from low temperatures (−30°C) to high temperatures (50°C). As a demonstration of its dual responsiveness, 16 pieces of RSF/AgNW/Ca(II) ionotronic skin were combined to make a 4 × 4 array. It demonstrated high sensitivity without interference between the pressure and temperature signals, achieving a significant dual response. A potential application for the simultaneous detection of body temperature and heartbeat was demonstrated by placing the RSF/AgNW/Ca(II) ionotronic skin on the wrist and further indicated the practicality of such an ionotronic skin because it could distinguish between the percussion wave, tidal wave, and diastolic wave in a single waveforms. Therefore, this RSF/AgNW/Ca(II) ionotronic skin that can discriminated between stimuli and work at low temperatures may have great potential in the field of wearable health monitoring equipment.

1. Introduction

As an important platform for the human body to interact with the outside world, skin has a variety of sensing functions so that people can process complex environmental information, such as pressure, temperature, and humidity [1–3]. Inspired by the sensing functions of skin, researchers have developed various sensing devices to achieve many features, like multiple responsiveness [4–5], high sensitivity [6], good flexibility [7], self-repair [8], and even self-powered functions [9]. However, the discrimination between different signals is still a weakness of multi-responsive sensing devices [10], because the effects of various stimuli often confuse and distort the signal [11].

In recent years, researchers have developed several flexible and highly sensitive pressure sensing electronic skins based on different sensing technologies, such as compression resistance, piezoelectricity, and capacitance [12–19]. Compression resistance electronic skins have a good response to both dynamic and static pressure stimulation. In addition, the device integration and signal monitoring are also relatively simple, so it has more applications than piezoelectricity and capacitance electronic skins [12,20]. Designing a surface microstructure on the selected electronic skin material that is inspired by the fingerprint structure on human beings has been suggested as a powerful means to

* Corresponding author.
E-mail address: chenx@fudan.edu.cn (X. Chen).
[1] These authors contributed equally: Qianying Chen, Hao Tang.

https://doi.org/10.1016/j.cej.2021.130091
Received 30 January 2021; Received in revised form 30 March 2021; Accepted 23 April 2021
Available online 28 April 2021

improve the sensing sensitivity [21]. In addition to traditional silicon stencils [20], microstructures originating from other common items also can be used to achieve similar sensitivity. For instance, Nie et al. fabricated a pressure sensing electronic skin by replicating the hierarchical microstructure of banana leaf that exhibited a high sensitivity (10 kPa^{-1}) and excellent durability (10,000 cycles) [22]. Wang et al. used the microstructure of a silk fabric to successfully develop a large-area, uniform, and flexible pressure sensing electronic skin [21]. Therefore, it is possible produce the low-cost, high-sensitivity, and large-scale pressure sensing materials using microstructures from the texture of common items.

In addition to pressure response, real-time and accurate responses to the temperature of the surrounding environment and objects are also an important capability of sensors [23,24]. Among the high-performance temperature sensors, silicon materials are still most commonly used [25,26]. Meanwhile, conductive polymers [27] and their composites [28–30] have also been suggested as temperature sensors to reduce the dependence on semiconductor materials and meet the flexibility requirements of the device. However, the sensitivity of these percolation-type sensors prepared from conductive polymer composites is not high enough [28]; and more importantly, most of them cannot work at low temperatures, which greatly limits their applications [30].

In general, synthetic polymers are the main material used to produce current temperature sensors because of their good processibility and mechanical properties [23,31]. However, considering that wearable sensors are frequently interfaced with skin, natural polymers that are biocompatible and have skin affinity have unique advantages [32–37]. For instance, You et al. [35] produced a biologic nanosheet from marine chitin that was expected to be desirable in wearable electronics, biodegradable circuits, and biologic devices. Lv et al. [36] reported a naturally-derived wearable strain sensor based on milk protein and natural rubber to avoid environmental pollution and improve biocompatibility.

Silk fibroin, a natural polymer derived from the *Bombyx mori* (*B. mori*) silkworm cocoon, is a good candidate for the matrix of an electronic skin because of its tunable processability and physical properties, such as the mechanical, optical, and thermal properties, as well as its unique advantages including biocompatibility, biodegradability, and bioabsorption [32,38–42]. In our previous work, we successfully developed an ionotronic skin for temperature sensing from a regenerated silk fibroin (RSF) hydrogel and calcium chloride ($CaCl_2$) that could be used below freezing point [43]. Herein, we use the same component but different preparation method to produce a more robust RSF/Ca(II) hydrogel as the matrix for temperature sensing and add a microstructured silver nanowires (AgNWs) conductive layer to the hydrogel surface to also achieve functionality as a pressure sensor [37]. Therefore, such a RSF/AgNWs/Ca(II) hydrogel could respond to both pressure and temperature and could be assembled into a pressure and temperature sensing bimodal ionotronic skin.

2. Experimental section

2.1. Materials

B. mori silkworm cocoons were procured from local farmers at Nantong, China. Sodium bicarbonate ($NaHCO_3$), sodium dodecyl sulfate (SDS), anhydrous calcium chloride ($CaCl_2$), and polyethylene glycol (PEG-20000) were purchased from Sinopharm Chemical Reagent Co. Ltd., Shanghai, China. Lithium bromide (LiBr) was obtained from Kuling Fine Chemical Co. Ltd., Shanghai, China. Dialysis tubes (MWCO: 12–14 kDa) were purchased from Blue Bird Co. Ltd., Shanghai, China. Silver nanowire (AgNW) aqueous solution (S40) was purchased from Cold Stone Nanomaterials Technology Co. Ltd., Suzhou, China. The diameters and lengths of the AgNWs were 40 ± 5 nm and 30 ± 5 μm, respectively. All chemicals used in this work were of analytical grade and used without further purification.

2.2. Preparation of RSF aqueous solution

The RSF aqueous solution was prepared from *B. mori* silkworm cocoons following a well-established procedure comprised of degumming, dissolving, and dialysis steps [44]. Briefly, the cocoons were first degummed by boiling in a 0.5 wt% $NaHCO_3$ twice for 30 min each time. After washing and drying, the degummed silk was then dissolved in 9.5 $mol{\cdot}L^{-1}$ LiBr aqueous solution by heating to 60°C for 1 h. Then, the solution was dialyzed against deionized water for 3 days with a dialysis tube (MWCO: 12–14 kDa) to remove the salt, and the RSF solution was acquired (silk fibroin concentration of approximately 5 wt%). The 5 wt % RSF aqueous solution was put into the 10 wt% PEG aqueous solution with a dialysis tube (MWCO: 12–14 kPa) to concentrate to the final fibroin concentration to approximately 15 wt%, and the solution was stored at 4°C until use.

2.3. Preparation of RSF/AgNW/Ca(II) hydrogel

Three kinds of RSF hydrogels with AgNWs embedded on the surface were prepared, including a control sample without microstructure and two samples with different microstructures on the surface. When preparing the control sample, 5 mL of 1 $mg{\cdot}mL^{-1}$ AgNW aqueous solution was poured onto the bottom of a 5 cm × 10 cm glass container and put in a 40°C oven to form a thin and homogeneous AgNW layer. When preparing the samples with microstructured surfaces, high density or low density cotton fabrics were first placed on the bottom of the glass mold. Then, the procedure was the same as that used for the control sample, and thin and homogeneous AgNW layer was formed on the cotton fabric.

An appropriate amount of SDS solution was added to the RSF solution to obtain a RSF/SDS mixed solution with a final silk fibroin concentration of 10 wt% and a SDS concentration of 20 $mmol{\cdot}L^{-1}$. The RSF/SDS solution was gently casted onto the bottom of the glass container that contained the deposited AgNWs. The glass container was heated in a 60°C oven for 30 min to form the RSF/AgNW hydrogel. The RSF/AgNW hydrogel was gently peeled off the bottom of the glass container. Finally, the RSF/AgNW hydrogel was first immersed in deionized water for 3 days to remove the uncombined SDS and then immersed in a $CaCl_2$ aqueous solution (10, 20, and 30 wt%) for 5 days to produce the final RSF/AgNW/Ca(II) hydrogels.

2.4. Assembly of RSF/AgNW/Ca(II) bimodal ionotronic skin

Two pieces of RSF/AgNW/Ca(II) hydrogel were stacked with the AgNW layers face-to-face. As shown in Scheme 1, a copper wire was mounted on the end of the AgNW layer of one RSF/AgNW/Ca(II) hydrogel as an electrode, but could not contact the AgNW layer of the other hydrogel. Then, two copper wires from the opposite AgNW layers were used as a pair of electrodes for subsequent pressure sensing tests. Meanwhile, two copper wires were mounted on the two ends of the matrix of the same RSF/AgNW/Ca(II) hydrogel layer to form a pair of electrodes for subsequent temperature sensing tests. Finally, two pieces of RSF/AgNW/Ca(II) hydrogel were fixed by soft tapes at their edges to prevent the slippage from each other.

2.5. Characterization

The mechanical properties of the hydrogel were performed on a universal testing machine (Instron5566, Instron, UK). The surface morphology was observed under a scanning electron microscope (TS5136MM, TESCAN, Czech). The conductivity of the hydrogel was calculated from the current–voltage (I–V) curve recorded with an electrochemical workstation (CHI660E, Chenhua Instrument Co. Ltd., China).

Pressure sensing tests consisted of following steps: the dynamometer (M5-012, Mark-10) was fixed on the moving subassembly and collected the pressure loading applied on the RSF/AgNW/Ca(II) ionotronic skin in

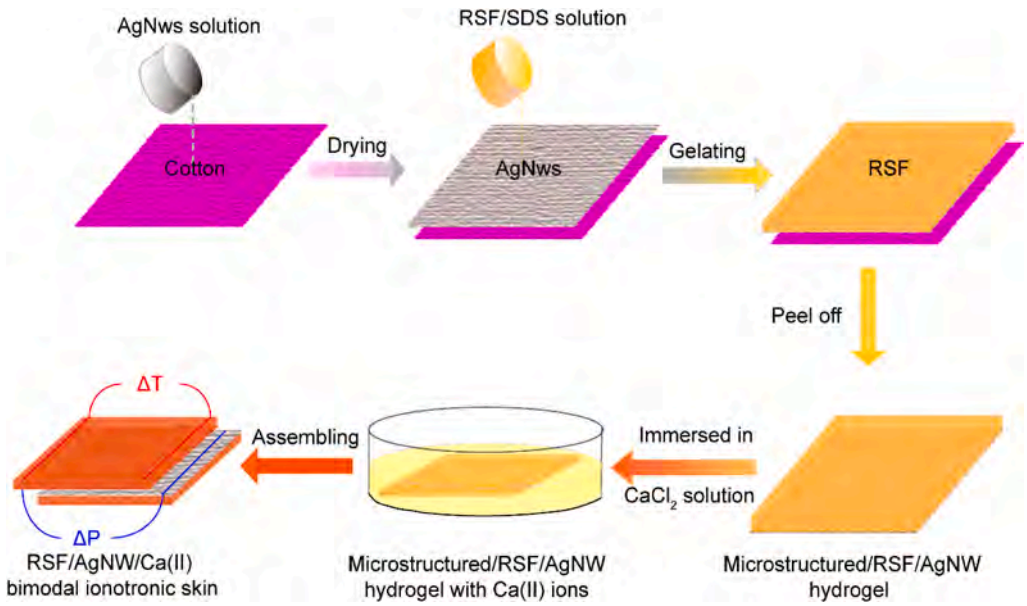

Scheme 1. Schematic for the preparation of RSF/AgNW/Ca(II) bimodal ionotronic skin.

real-time with vertical movements of the testing machine (CMT6103, MTS Systems). Meanwhile, the real-time current signal corresponding to the pressure loading was recorded by the electrochemical workstation (PARSTA2273, Princeton Applied Research). The cyclic loading was provided by a motion controller (DZ100MA00, well known). The sensitivity (S) of the pressure sensor was defined as follows:

$$S = \frac{\delta(\Delta I/I_0)}{\Delta P} \quad (1)$$

where ΔI is the amount of current change, I_0 is the initial current without pressure, and ΔP is the amount of pressure change.

Temperature sensing tests were performed with a temperature-controlled stage (THMS600, Linkam, UK). During the temperature change, the resistance changes of the RSF/AgNW/Ca(II) ionotronic skin were recorded in real-time using the electrochemical workstation (CHI660E, Chenhua Instrument Co. Ltd., China). The sensitivity of the temperature sensing was defined as follows:

$$S = \frac{\delta(\Delta R/R_0)}{\Delta T} \quad (2)$$

where ΔR is the amount of resistance change, R_0 is the resistance at 0°C, and ΔT is the amount of temperature change.

3. Results and discussion

3.1. Preparation and characterization of RSF/AgNW/Ca(II) hydrogels

The preparation steps of the RSF/AgNW/Ca(II) hydrogel are shown in Scheme 1. Herein, cotton fabric was used as the template to generate the microstructure on the surface of RSF hydrogel. The advantage for choosing cotton fabric is that it is cheaper and more suitable for mass production than other materials [22–23]. AgNWs were first deposited on the cotton fabric and then transferred to the RSF hydrogel surface during the hydrogel formation process. The strategy for the preparing the RSF/Ca(II) hydrogel was different in this study than reported in our previous work [43] and other research groups [45]. First, by adding a small amount of sodium dodecyl sulfate (SDS) to the RSF aqueous solution, a robust and elastic RSF hydrogel could be obtained according to our previous work [46]. Therefore, the AgNW-containing microstructure could be formed on the hydrogel surface during the gelation process. Then, the formed RSF/AgNWs hydrogel was saturated in an aqueous $CaCl_2$ solution to introduce Ca(II) ions into the hydrogel and created a RSF/AgNWs/Ca(II) hydrogel that was sensitive to both temperature and pressure. The reason to choose soaking the RSF hydrogel in the $CaCl_2$ solution instead of adding $CaCl_2$ in RSF aqueous solution before the formation of the hydrogel is because the mechanical properties of the RSF hydrogel by the later preparation method were rather weak [43,45,47]. Herein, a robust and elastic RSF hydrogel is needed as the matrix to build up the pressure sensor, so the Ca(II) ions were introduced to the hydrogel network after the strong RSF hydrogel was formed by adding SDS in the preparation procedure. It is worth noting that preparation method for the RSF hydrogel by the addition of SDS was well established and the formation mechanism and other information (such as biocompatibility) can be found in our previous work [46] and the reference cited there [48].

Fig. 1a–c shows the integration of AgNWs on the surface of the RSF hydrogel. Interconnected AgNWs on the surface of the RSF hydrogels would provide a conductive layer for the designed pressure sensing ionotronic skin regardless of whether or not they have microstructure. Two kinds of cotton fabrics (low-density and high-density) were used to create a microstructured AgNW surface on the RSF hydrogel. No matter which kind of cotton fabric was used, the warp and weft interlaced weaving process gives the surface a highly repeating concave and convex pattern. Meanwhile, as each strand used in weaving is composed of many cotton threads, the surface of each strand displays a further subtle pattern (insets of Fig. 1b and 1c). Fig. 1b and 1c clearly demonstrate the microstructures formed on the RSF hydrogels using low-density and high-density cotton cloth as a template. Moreover, the small gap between the cotton threads in each strand of the cloth was also reproduced within the hydrogel grooves (Fig. S1). Therefore, by using the method shown in Scheme 1, different levels of cotton fabric microstructures were almost completed engraved into the surface during the hydrogel formation process. In addition, the resulting RSF hydrogel was quite robust and elastic and was easy to peel off from the cotton fabric while perfectly maintaining the delicate pattern on the surface. Such a hierarchical microstructure may provide great possibilities for the ionotronic skin to have a high pressure sensitivity [49].

The conductivity of the RSF hydrogel was due to the Ca(II) ions trapped in the hydrogel network, thus the mass and conductivity RSF hydrogels upon soaking the materials in different aqueous $CaCl_2$ solution were extensively studied. Fig. 1d indicates that the weight of the RSF hydrogel decreased slightly after immersion in deionized water

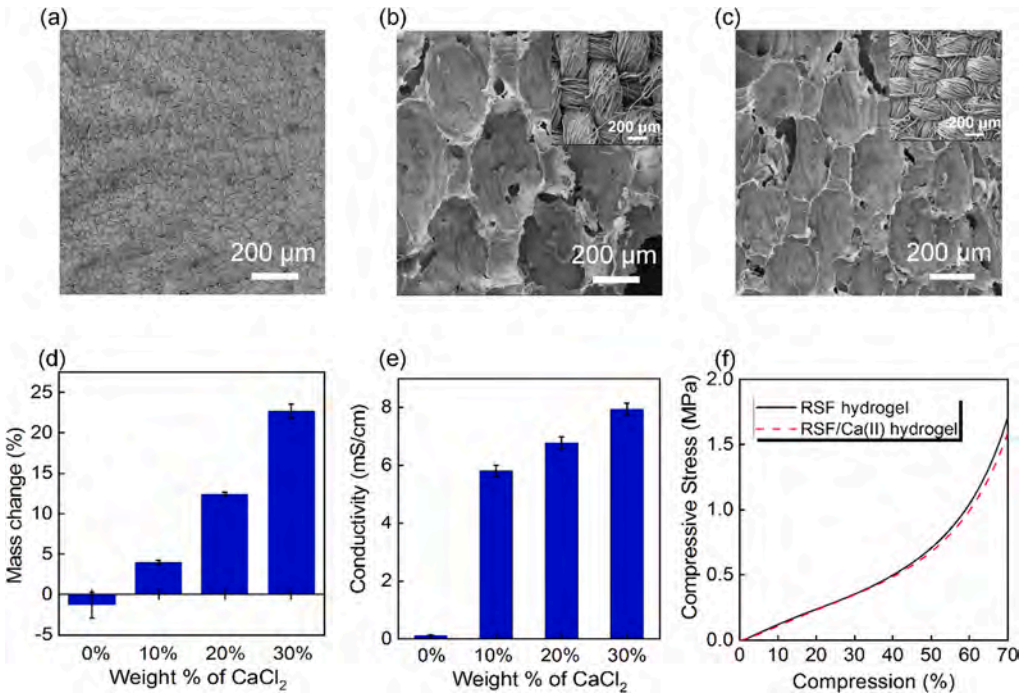

Fig. 1. (a – c) SEM images of the microstructures on the surface of the RSF/AgNW/Ca(II) hydrogels. (a) Without template, (b) using low density cotton fabric as the template, and (c) using high density cotton fabric as the template (the inset of (b) and (c) shows the corresponding texture of the cotton fabrics). (d) Effect of $CaCl_2$ concentration on the mass change of RSF/AgNW/Ca(II) hydrogels. (e) Effect of $CaCl_2$ concentration on the conductivity change of RSF/AgNW/Ca(II) hydrogels. (f) Comparison of the compression curves of RSF/AgNW/Ca(II) hydrogels ($CaCl_2$ concentration was 30 wt%).

(about 1.3%), mainly due to the removal of free SDS from the hydrogel. However, the weight of the RSF hydrogels after soaking in the $CaCl_2$ solutions increased significantly. The weight of RSF hydrogel immersed in 10 wt%, 20 wt%, and 30 wt% aqueous $CaCl_2$ solutions increased by 4.0%, 12.4%, and 22.7%, respectively. However, if the RSF hydrogel was immersed in 40 wt% aqueous $CaCl_2$ solution, it was integrated overnight (Fig. S2) because the high concentration of Ca(II) ions would destroy the RSF hydrogel network. Therefore, 30 wt% was the highest concentration of the aqueous $CaCl_2$ solution used in this study.

The increase of weight could be attributed to the incorporation of Ca (II) ions in the RSF hydrogel, and the conductivity of the RSF hydrogel also increased with increasing Ca(II) incorporation (Fig. 1e). Compared to the pristine RSF hydrogel that was almost non-conductive (conductivity of only 0.1 $mS{\cdot}cm^{-1}$, Table S1), the conductivity of the RSF hydrogel soaked in a 30 wt% $CaCl_2$ solution reached 7.9 $mS{\cdot}cm^{-1}$, which was quite a good conductive property.

Although the weight and the conductivity changed significantly after soaking in the 30 wt% $CaCl_2$ aqueous solution, the mechanical properties of the RSF hydrogel remained mostly unchanged. Fig. 1f shows that the compression curves of the two RSF hydrogel samples (pristine and after immersion in the 30 wt% $CaCl_2$ aqueous solution) were very close. The linear deformation region of both samples was very wide (up to ~35%) and the compression modulus was around 1.0 MPa (Table S1). This result was understandable because the Ca(II) ions were trapped in the RSF hydrogels network which had little effect on the mechanical performance. The tensile test of these two samples were also performed (Fig. S3). The results showed that the hydrogels were quite stiff, but the less extensibility did not affect their application as the pressure sensors.

In addition, the introduction of Ca(II) into the network of the RSF hydrogels had the advantage for keeping the hydrogel stable in an open environment. Fig. S4 compares the states of the pristine RSF hydrogel and the hydrogel soaked in the 30 wt% $CaCl_2$ aqueous solution after they were put on a conductive silver film in moderate humidity (~50% RH). After 12 h, the RSF hydrogel immersed in deionized water and 10 wt% $CaCl_2$ aqueous solution dried, shrank significantly, and broke away from the conductive silver layer. The shrinkage of the RSF hydrogel immersed in the 20 wt% $CaCl_2$ aqueous solution was much less, and the sample immersed in the 30 wt% $CaCl_2$ aqueous solution was almost unchanged. Fig. S5 shows after being placed in a relatively dry (50% R.H.) open environment for 14 days, the weights of the RSF/Ca(II) hydrogels were almost unchanged, further indicating their good stability in an open environment. Therefore, considering the conductivity, mechanical performance, and stability in the ambient environment, the RSF/Ca(II) hydrogel soaked in 30 wt% $CaCl_2$ aqueous solution was selected to prepare the matrix and the temperature sensing portion of the bimodal ionotronic skin.

3.2. *Pressure sensitivity of RSF/AgNW/Ca(II) hydrogels*

As shown in Scheme 1, two pieces of RSF/AgNW/Ca(II) hydrogel (with thickness about 1.8 mm) were assembled into a pressure sensor by facing the AgNWs conductive layers towards each other. Fig. 2a shows the change in current signal of the three pressure sensors made from the RSF/AgNW/Ca(II) hydrogels with different surface microstructures when different pressures were applied. There was almost no current change when different pressure was applied on the RSF/AgNW/Ca(II) pressure sensor without a surface microstructure. However, for both RSF/AgNW/Ca(II) pressure sensors with surface microstructures, the current changed significantly when the pressure changed, suggesting they had a good response to the applied pressure. In the initial state, the top and the bottom AgNW layer contacted with each other, forming the conductive paths. Hierarchical microstructure led to uneven conductive surfaces, decreasing the areas of the contacting part. Therefore, less conductive paths were formed in the pressure sensor with surface microstructures compared to that without a surface microstructure. When pressure applied, the contact area between the two AgNW layers increased, so the conductive paths increased and thus the current also increased. For the pressure sensor with surface microstructures, the change of conductive paths was much more significantly than that without a surface microstructure, so the current changes also varied dramatically, showing a sensitive response to the pressure applied. The current change when the pressure released was also monitored. There was a small hysteresis between the pressure increasing and decreasing process (Fig. S6a), which was certainly come from the resilient hysteresis of the hydrogel when the applied pressure was released (Fig. S6b). However, this would not affect the work of the pressure sensor as in most case, only the signals generated with applied pressure needed to be recorded.

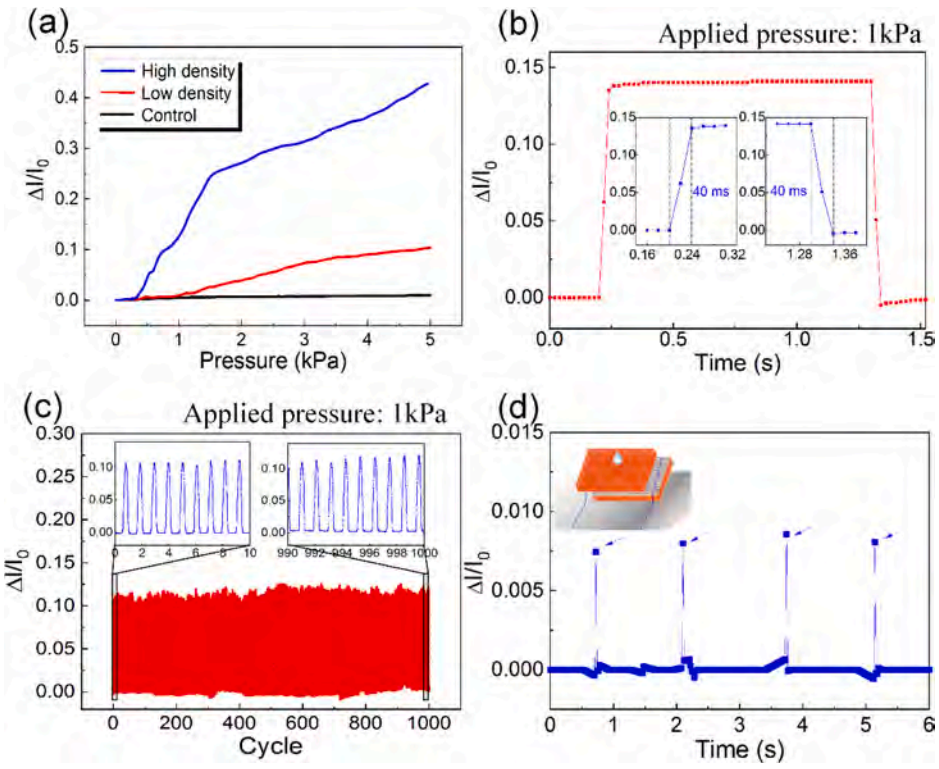

Fig. 2. Performance of the RSF/AgNW/Ca(II) pressure sensor. (a) Relative change in current ($\Delta I/I_0$) versus applied pressure. (b) Response curve at an applied pressure of 1 kPa. (c) Durability test by performing 1000 loading–unloading cycles at a frequency of 1 Hz under an applied pressure of 1 kPa. The inset shows an enlarged view, exhibiting a highly reliable and stable sensing performance. (d) Real-time current changes to falling water droplets. The inset shows the schematic for water dropping test.

The working range of the RSF/AgNW/Ca(II) pressure sensor was 0.3–5 kPa. In particular, the sample with the more complicated microstructure (i.e., using high-density cotton fabric as template) showed a higher sensitivity. The sensitivity reached 0.20 kPa^{-1} when the applied pressure ranged from 0.3 to 1.5 kPa. Although the sensitivity decreased when the applied pressure further increased (from 1.5 to 5.0 kPa), it still had a sensitivity of 0.05 kPa^{-1} which was comparable to previously reported data [6,12,50].

The response time of the pressure response is shown in Fig. 2b. When the assembled RSF/AgNW/Ca(II) hydrogels were loaded and unloaded with a pressure of 1 kPa, the response and release times were both found to be 40 ms, which is equivalent to or even better than the pressure sensors reported in the literature [4,10,51]. The durability of the RSF/AgNW/Ca(II) pressure sensor was evaluated by applying 1000 loading/unloading cycles at a pressure of 1 kPa and a frequency of 1 Hz. The result showed that the pressure sensing of the RSF/AgNW/Ca(II) hydrogel had good reliability and reproducibility with negligible hysteresis (Fig. 2c). In addition, the performance of the pressures sensor when applying at the pressure from 1.5 kPa to 2 kPa (Fig. S7a) as well as increasing the number of the loading/unloading cycles to 3000 (Fig. S7b) were also tested, and both results indicated that RSF/AgNW/Ca(II) pressure sensor still showed a fairly good reliability and reproducibility. Compared with other sensors made from supramolecular hydrogels [8], metal substrates [52], and graphene composites [53] with encapsulation layers to improve the sensor stability in harsh environments, the stability RSF/AgNW/Ca(II) pressure sensor studied here was significantly improved because of Ca(II) ions improved the water retention in the hydrogel [51,54,55].

To investigate the ability of the RSF/AgNW/Ca(II) pressure sensor to detect a subtle change in pressure, the thickness of the RSF/AgNW/Ca(II) hydrogel was reduced to 0.75 mm. As shown in Fig. 2d, the pressure sensor was able to detect water drops timely and sensitively when a water drop of approximately 20 mg was used to simulate rainfall from a height of approximately 10 cm. The current increased suddenly when the water drop hit the pressure sensor as indicated by the arrow in the figure.

3.3. Temperature sensitivity of RSF/AgNW/Ca(II) hydrogels

For an ionic conductor, changes in temperature affect the movement of ions. As for RSF/AgNW/Ca(II) hydrogel, there was about 90 wt% of water, therefore a large number of water molecules provided channels for the migration of Ca(II) ions. The interactions between the Ca(II) ions and the water molecules, as well as the silk fibroin chain segments were highly temperature dependent. Accordingly, the movement of the Ca(II) ions in the RSF/AgNW/Ca(II) hydrogel varied with temperature which meant that the electrical signal from the hydrogel responded to temperature changes. As we shown in our previous work [43], RSF/Ca(II) hydrogel still kept flexible at −30°C because the existence of the $CaCl_2$ significantly decreased the freezing point of water. It is not surprised that freezing point of water decreased in $CaCl_2$ solution as Conde et al. reported the freezing point of 30 wt% $CaCl_2$ solution was below −40°C [56]. In addition, Morelle et al. demonstrated a tough polyacrylamide-alginate double network hydrogel that can be cooled down to the temperature as low as −57°C without freezing by adding a suitable amount of $CaCl_2$ [57]. Therefore, the RSF/AgNW/Ca(II) hydrogel prepared in this study maintain the good anti-freezing properties, endow the temperature sensor have a wide working temperature range at least from −30 to 50°C. When the temperature increased, the resistance of the RSF/AgNW/Ca(II) hydrogel decreased, and vice versa (Fig. 3a). Thus, the slope of the linear fit to the rate of resistance versus the change in temperature in Fig. 3a represents the sensitivity of such a temperature sensor. The sensitivity of the RSF/AgNW/Ca(II) hydrogel was approximately 5.02%°C^{-1} over a temperature range of −30–0°C and 1.54%°C^{-1} over a temperature range of 0–50°C. The sensitivity at both low and high temperatures were higher than those of other hydrogel-based ionotronic skin materials reported in the literature prepared by using similar methods (Table S2).

Fig. 3b shows the high sensitivity and signal stability of the RSF/AgNW/Ca(II) hydrogel to temperature changes with a resolution as small as 0.5°C or 1.0°C. However, it was still hard for us to obtain the data with a resolution as small as 0.1°C due to the limitation of the temperature-controlled stage (the highest resolution is 0.5°C).

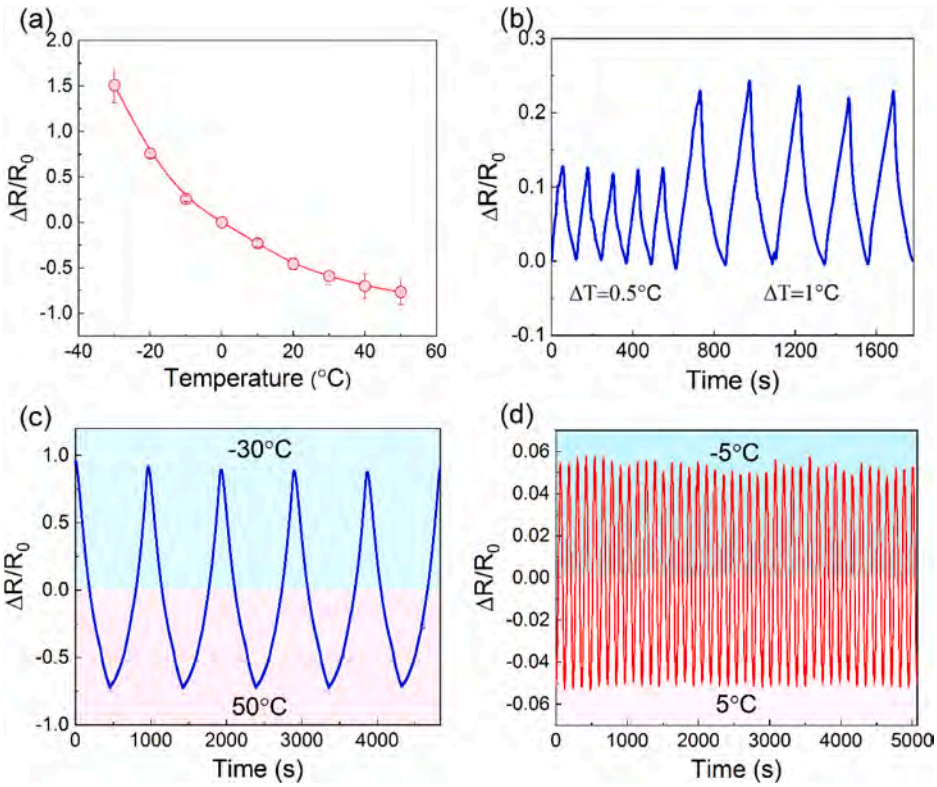

Fig. 3. Performance of the RSF/AgNW/Ca(II) hydrogel temperature sensor. (a) Resistance change at different temperature. (b) Resistance change cycles in response to slight temperature changes. (c) Resistance change after 5 cyclic temperature changes from − 30°C to 50°C. (d) Resistance change after 50 cyclic temperature changes from − 5°C to 5°C.

Therefore, it is not possible for us to say very confidently that resolution of such a temperature sensor is enough for testing the body temperature (which needs 0.1°C resolution). On the other hand, the sensitivity of the RSF/AgNW/Ca(II) temperature sensor was 1.54%°C^{-1} over a temperature range of 0–50°C, which is similar to that of Trung's work (1.34%°C^{-1}) reported in the literature [23], where they demonstrated the successful application for the detection on body temperature. Thus, we believe the RSF/AgNW/Ca(II) temperature sensor has the great potential for the detection of body temperature. In addition, the effectiveness of the RSF/AgNW/Ca(II) hydrogel as a temperature sensor at −30°C and 50°C was examined (Fig. 3c). The results showed that at these two extreme operating temperatures, the RSF/AgNW/Ca(II) hydrogel still maintained its temperature sensitivity, showing a consistent resistance variation amplitude over five cycles. More specifically, the resistance changes of the RSF/AgNW/Ca(II) hydrogel were very stable around the freezing point of water (−5 to 5°C, Fig. 3d). Therefore, the temperature sensing ionotronic skin made from RSF/AgNW/Ca(II) hydrogel not only exhibited a wide working range, but also had a high sensitivity. The hydrogel could be considered an ideal skin sensing system for applications in extreme temperature environments, especially at very low temperatures which are difficult for most temperature sensors, especially electronic skins [23,29,58–61].

3.4. Performance of simultaneous sensing RSF/AgNW/Ca(II) bimodal ionotronic skin

On the basis of the instinct biocompatibility and skin-friendly properties of silk fibroin and the good pressure and temperature sensitivity of the RSF/AgNW/Ca(II) hydrogels shown above, they could also act as a bimodal ionotronic skin that simultaneously responds to pressure and temperature. In our previous work, it has been proved that the RSF hydrogel made by the addition of SDS had no serious cytotoxicity [46] and other research groups also proved that no skin inflammation was found when the RSF electrodes or the adhesives containing high concentration of $CaCl_2$ were attached on the skin [47,62]. Fig. 4a–c shows the electrical signals of the RSF/AgNW/Ca(II) bimodal ionotronic skin under different pressure and temperature conditions. When an empty beaker was placed on the bimodal ionotronic skin, only the pressure sensing current increased in response to the weight of the beaker (8.20 g), and there was no change in the measured resistance related to the temperature sensing because there was no change in temperature (Fig. 4a). However, when 50°C hot water was poured into the beaker, electrical signals for both pressure and temperature sensing were measured. The current due to the pressure sensing increased from the increased weight of the beaker with water (total weight 12.00 g), and the resistance due to the temperature sensing decreased due to the increase in temperature from the hot water (Fig. 4b). Similarly, the electrical signals of the RSF/AgNW/Ca(II) bimodal sensing ionotronic skin varied due to the pressure and temperature change when the beaker contained 0°C water (Fig. 4c).

After testing the bimodal sensing of a single piece of RSF/AgNW/Ca(II) bimodal sensing ionotronic skin, a 4 × 4 pixels sensing array was assembled by 16 pieces of 10 × 10 mm RSF/AgNW/$CaCl_2$ ionotronic skins. In the array, each ionotronic skin remained independent, and the pressure and temperature sensed on each pixel were monitored in real time. During the test, a relatively heavy serum bottle filled with hot water (total weight 4.5 g, 50°C) and a relatively light serum bottle containing a small amount of cold water (total weight 3.5 g, 0°C) were placed on two different ionotronic skin pixels (Fig. 4d and Fig. S8). The pressure and temperature map of the RSF/AgNW/Ca(II) sensing array are shown in Fig. 4e and 4f. The results clearly demonstrated that when the 4 × 4 pixels RSF/AgNW/Ca(II) sensing array was used to monitor the pressure, the current intensity increased significantly at the location where the serum bottle was placed, and the increase was proportional to the magnitude of the pressure (Fig. 4e). For the temperature monitoring, the measured resistance from where the hot serum bottle was placed

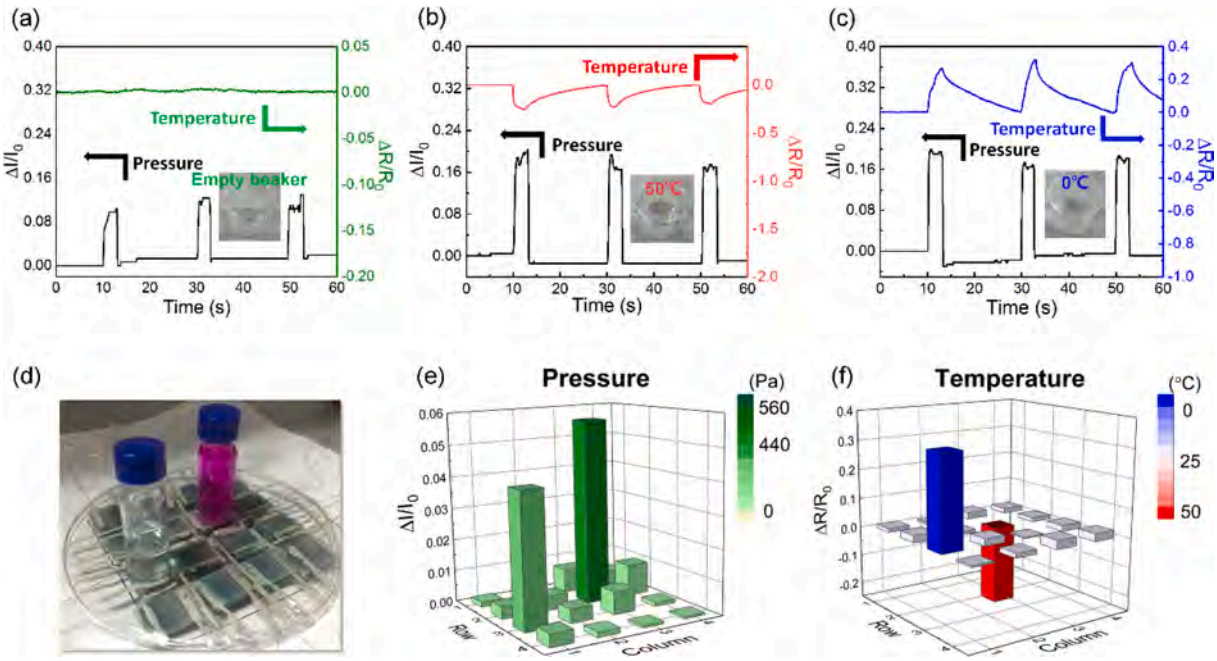

Fig. 4. Simultaneous sensing performance of the RSF/AgNW/Ca(II) bimodal ionotronic skin. Pressure and temperature sensing responses to (a) an empty beaker, (b) hot water in the beaker (50°C), and (c) cold water in the beaker (0°C) (weight of beaker: 8.20 g; weight of beaker and water: 12.00 g). (d) Photograph of the bimodal ionotronic skin array with 4 × 4 pixels and two vials with different weights and temperatures and the corresponding results in (e) pressure and (f) temperature detection. (The serum bottle with red liquid: 4.5 g, 50°C; the serum bottle with blue liquid: 3.5 g, 0°C). (For interpretation of the references to colour in this figure legend, the reader is referred to the web version of this article.)

significantly decreased and increased where the cold serum bottle placed (Fig. 4f). The demonstrations shown in Fig. 4e and 4f clearly indicate that the pressure and temperature sensing signals in the RSF/AgNW/Ca(II) sensing array were independent and truly reflected information about the pressure and temperature of the test object. Therefore, the RSF/AgNW/Ca(II) ionotronic skin ensured a mutual response to both the pressure and temperature signals and achieved a bimodal response effect.

As practical application of the RSF/AgNW/Ca(II) bimodal ionotronic skin, it was attached to a person's wrist (Fig. 5a) and used to detect changes in body temperature and the heartbeat spontaneously. It is easy to imagine how the ionotronic skin could be used to detect body temperature according to the demonstration shown above (Fig. 3). However, the real-time periodic arterial pulse waveforms detected by the

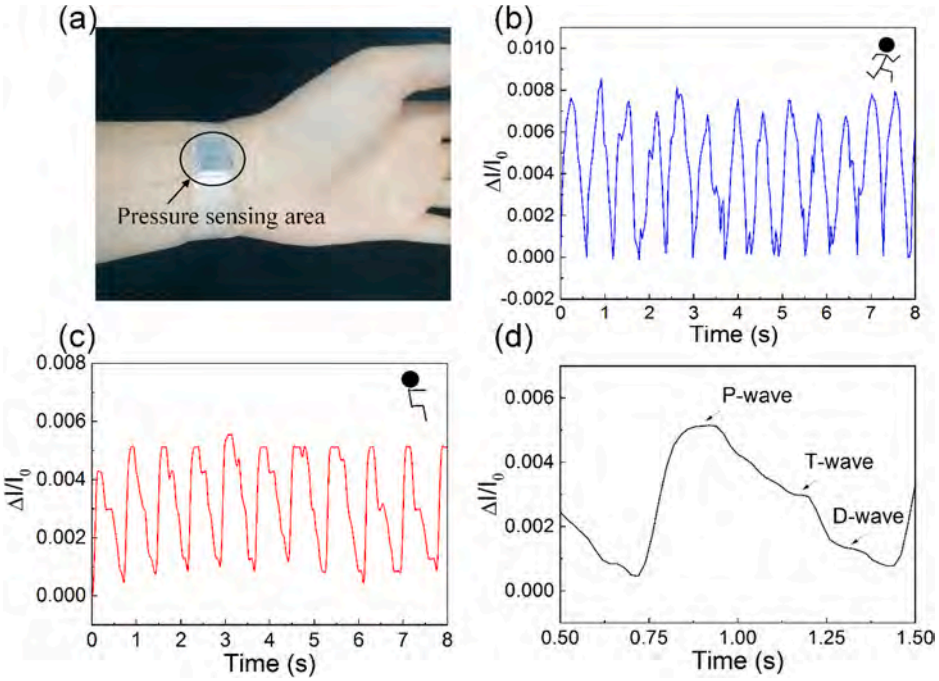

Fig. 5. (a) Photograph of the ionotronic skin attached to the wrist for detecting artery pulses, real-time current changes in response to artery pulse pressure after exercise (b) and in relaxation (c), Waveform of a single pulse (d) extracted from (c).

RSF/AgNW/Ca(II) ionotronic skin undoubtedly highlighted its flexible wearability and considerable sensibility. Fig. 5b and 5c shows a typical radial arterial pulse waveform within 8 s after exercise and in relaxation, equivalent to 99 and 75 beats per minute respectively. In addition, most of the recorded radial arterial pulse waveforms had three clearly distinguishable peaks, that is, the percussion wave (P–wave, P_1), tidal wave (T–wave, P_2), and diastolic wave (D–wave, P_3) as shown in Fig. 5d. The radial augmentation index AI_r (P_2/P_1) is an important value for characterizing arterial stiffness and can be obtained from these data [63]. The calculated AI_r value was about 0.56, which was a characteristic value for a healthy adult female [64]. Moreover, the RSF/AgNW/Ca(II) ionotronic skin could detect the D-wave in the arterial pulse waveform that the majority of other electronic skins used in arterial tonometry cannot detect [2,52,65,66], and thus has great potential for use in more detailed diagnostics. However, the three kinds of waves seemed not clearly distinguishable after the exercise. The disappearance of the T-wave after exercise may be caused by exercise-induced vasodilation, dilation of muscular arteries, and enhanced ventricular–vascular coupling [67]. In addition, the heart beats faster and stronger after exercise, so the intensity of P-wave becomes more significantly, which may suppress the intrinsic weaker T-wave and D-wave. Similar phenomenon also can be found in the literature [3,65,68].

4. Conclusion

Herein, a silk-based bimodal ionotronic skin was created by assembling two pieces of RSF/AgNW/Ca(II) hydrogel face-to-face. First, the robust RSF hydrogels were prepared by adding SDS, a method previously developed in this laboratory. During the RSF hydrogel formation process, a thin and conductive AgNW layer was embedded on the microstructured hydrogel surface created by using cotton fabric as a template. Then, the RSF/AgNW hydrogel was soaked in a $CaCl_2$ aqueous solution to endow the whole RSF hydrogel conductivity and form the final RSF/AgNW/Ca(II) hydrogel. As a pressure sensor, the sensitivity of the RSF/AgNW/Ca(II) ionotronic skin reached as high as 0.20 kPa^{-1} because of the introduction of the microstructure on the RSF hydrogel surface. As a temperature sensor, the RSF/AgNW/Ca(II) ionotronic skin achieved a sensitivity of 1.54%°C^{-1} over a temperature range 0–50°C. More impressively, the RSF/AgNW/Ca(II) ionotronic skin also worked in a low temperature range (−30−0°C) with a high sensitivity of 5.02%°C^{-1}.

A dual response to pressure and temperature was achieved within a single RSF/AgNW/Ca(II) ionotronic skin. Afterwards, a 4 × 4 pixel sensing array was assembled from 16 pieces of RSF/AgNW/$CaCl_2$ ionotronic skins. The pressure and temperature signals from this sensing array were highly independent, indicating these signals would not interfere with each other in real application. As a demonstration of the possible application, a piece of RSF/AgNW/Ca(II) ionotronic skin was attached to a person's wrist to monitor his/her body temperature and heartbeat. Such an ionotronic skin not only could obtain the real-time periodic arterial pulse waveforms, but also could distinguish the percussion wave, tidal wave, and diastolic wave in a single waveform, which could be very useful for more detailed diagnostics. In addition, such a RSF/AgNW/Ca(II) ionotronic skin may also be applied in orthodontic treatment to detect the movements of the upper and lower jaws and the corresponding temperature changes in response to chewing. Considering the good biocompatibility and skin-friendly properties of silk fibroin, it is believed that this RSF/AgNW/Ca(II) ionotronic skin with dual response modes and high sensitivity has good application prospects in the field of wearable health monitoring equipment.

Declaration of Competing Interest

The authors declare that they have no known competing financial interests or personal relationships that could have appeared to influence the work reported in this paper.

Acknowledgment

This work was supported by the National Natural Science Foundation of China (Nos. 21935002, U2032123, and 21574023). We thank Dr. Bingjiao Zhao at Shanghai Stomatological Hospital, Fudan University for her valuable suggestions and discussions.

Appendix A. Supplementary data

Supplementary data to this article can be found online at https://doi.org/10.1016/j.cej.2021.130091.

References

[1] D. Chen, Q. Pei, Electronic muscles and skins: A review of soft sensors and actuators, Chem. Rev. 117 (17) (2017) 11239–11268, https://doi.org/10.1021/acs.chemrev.7b00019.
[2] K. Kim, M. Jung, B. Kim, J. Kim, K. Shin, O. Kwon, S. Jeon, Low-voltage, high-sensitivity and high-reliability bimodal sensor array with fully inkjet-printed flexible conducting electrode for low power consumption electronic skin, Nano Energy 41 (2017) 301–307, https://doi.org/10.1016/j.nanoen.2017.09.024.
[3] Q. Wang, M. Jian, C. Wang, Y. Zhang, Carbonized silk nanofiber membrane for transparent and sensitive electronic skin, Adv. Funct. Mater. 27 (9) (2017) 1605657, https://doi.org/10.1002/adfm.201605657.
[4] S.Y. Kim, S. Park, H.W. Park, D.H. Park, Y. Jeong, D.H. Kim, Highly sensitive and multimodal all-carbon skin sensors capable of simultaneously detecting tactile and biological stimuli, Adv. Mater. 27 (28) (2015) 4178–4185, https://doi.org/10.1002/adma.v27.2810.1002/adma.201501408.
[5] D.H. Ho, Q. Sun, S.Y. Kim, J.T. Han, D.H. Kim, J.H. Cho, Stretchable and multimodal all graphene electronic skin, Adv. Mater. 28 (13) (2016) 2601–2608, https://doi.org/10.1002/adma.201505739.
[6] J. Lee, H. Kwon, J. Seo, S. Shin, J.H. Koo, C. Pang, S. Son, J.H. Kim, Y.H. Jang, D. E. Kim, T. Lee, Conductive fiber-based ultrasensitive textile pressure sensor for wearable electronics, Adv. Mater. 27 (15) (2015) 2433–2439, https://doi.org/10.1002/adma.201500009.
[7] S. Lee, A. Reuveny, J. Reeder, S. Lee, H. Jin, Q. Liu, T. Yokota, T. Sekitani, T. Isoyama, Y. Abe, Z. Suo, T. Someya, A transparent bending-insensitive pressure sensor, Nat. Nanotechnol. 11 (5) (2016) 472–478, https://doi.org/10.1038/nnano.2015.324.
[8] Z. Lei, P. Wu, A supramolecular biomimetic skin combining a wide spectrum of mechanical properties and multiple sensory capabilities, Nat. Commun. 9 (2018) 1134, https://doi.org/10.1038/s41467-018-03456-w.
[9] K.-Y. Chun, Y.J. Son, E.-S. Jeon, S. Lee, C.-S. Han, A self-powered sensor mimicking slow- and fast-adapting cutaneous mechanoreceptors, Adv. Mater. 30 (12) (2018) 1706299, https://doi.org/10.1002/adma.v30.1210.1002/adma.201706299.
[10] S. Zhao, R. Zhu, Electronic skin with multifunction sensors based on thermosensation, Adv. Mater. 29 (15) (2017) 1606151, https://doi.org/10.1002/adma.201606151.
[11] J. Park, M. Kim, Y. Lee, H.S. Lee, H. Ko, Fingertip skin-inspired microstructured ferroelectric skins discriminate static/dynamic pressure and temperature stimuli, Sci. Adv. 1 (9) (2015) e1500661, https://doi.org/10.1126/sciadv.1500661.
[12] N. Luo, W. Dai, C. Li, Z. Zhou, L. Lu, C.C.Y. Poon, S.-C. Chen, Y. Zhang, N.i. Zhao, Flexible piezoresistive sensor patch enabling ultralow power cuffless blood pressure measurement, Adv. Funct. Mater. 26 (8) (2016) 1178–1187, https://doi.org/10.1002/adfm.v26.810.1002/adfm.201504560.
[13] M. Jian, K. Xia, Q.i. Wang, Z. Yin, H. Wang, C. Wang, H. Xie, M. Zhang, Y. Zhang, Flexible and highly sensitive pressure sensors based on bionic hierarchical structures, Adv. Funct. Mater. 27 (9) (2017) 1606066, https://doi.org/10.1002/adfm.201606066.
[14] T.Q. Trung, N.-E. Lee, Flexible and stretchable physical sensor integrated platforms for wearable human-activity monitoringand personal healthcare, Adv. Mater. 28 (22) (2016) 4338–4372, https://doi.org/10.1002/adma.v28.2210.1002/adma.201504244.
[15] M. Zhu, Y. Wang, M. Lou, J. Yu, Z. Li, B. Ding, Bioinspired transparent and antibacterial electronic skin for sensitive tactile sensing, Nano Energy 81 (2021), 105669, https://doi.org/10.1016/j.nanoen.2020.105669.
[16] M. Zhu, M. Lou, J. Yu, Z. Li, B. Ding, Energy autonomous hybrid electronic skin with multi-modal sensing capabilities, Nano Energy 78 (2020) 105208, https://doi.org/10.1016/j.nanoen.2020.105208.
[17] M. Zhu, M. Lou, I. Abdalla, J. Yu, Z. Li, B. Ding, Highly shape adaptive fiber based electronic skin for sensitive joint motion monitoring and tactile sensing, Nano Energy 69 (2020) 104429, https://doi.org/10.1016/j.nanoen.2019.104429.
[18] M. Lou, I. Abdalla, M. Zhu, J. Yu, Z. Li, B. Ding, Hierarchically rough structured and Self-Powered pressure sensor textile for motion sensing and pulse monitoring, ACS Appl. Mater. Inter. 12 (1) (2020) 1597–1605, https://doi.org/10.1021/acsami.9b1923810.1021/acsami.9b19238.s001.
[19] M. Lou, I. Abdalla, M. Zhu, X. Wei, J. Yu, Z. Li, B. Ding, Highly wearable, breathable, and washable sensing textile for human motion and pulse monitoring, ACS Appl. Mater. Inter. 12 (17) (2020) 19965–19973, https://doi.org/10.1021/acsami.0c0367010.1021/acsami.0c03670.s001.
[20] B. Zhu, Z. Niu, H. Wang, W.R. Leow, H. Wang, Y. Li, L. Zheng, J. Wei, F. Huo, X. Chen, Microstructured graphene arrays for highly sensitive flexible tactile

sensors, Small 10 (18) (2014) 3625–3631, https://doi.org/10.1002/smll.v10.1810.1002/smll.201401207.
[21] X. Wang, Y. Gu, Z. Xiong, Z. Cui, T. Zhang, Silk-molded flexible, ultrasensitive, and highly stable electronic skin for monitoring human physiological signals, Adv. Mater. 26 (9) (2014) 1336–1342, https://doi.org/10.1002/adma.201304248.
[22] P. Nie, R. Wang, X. Xu, Y. Cheng, X. Wang, L. Shi, J. Sun, High-Performance piezoresistive electronic skin with bionic hierarchical microstructure and microcracks, ACS Appl. Mater. Inter. 9 (17) (2017) 14911–14919, https://doi.org/10.1021/acsami.7b0197910.1021/acsami.7b01979.s001.
[23] T.Q. Trung, S. Ramasundaram, B.-U. Hwang, N.-E. Lee, An all-elastomeric transparent and stretchable temperature sensor for body-attachable wearable electronics, Adv. Mater. 28 (3) (2016) 502–509, https://doi.org/10.1002/adma.v28.310.1002/adma.201504441.
[24] C. Hou, H. Wang, Q. Zhang, Y. Li, M. Zhu, Highly conductive, flexible, and compressible all-graphene passive electronic skin for sensing human touch, Adv. Mater. 26 (29) (2014) 5018–5024, https://doi.org/10.1002/adma.201401367.
[25] R.C. Webb, A.P. Bonifas, A. Behnaz, Y. Zhang, K.J. Yu, H. Cheng, M. Shi, Z. Bian, Z. Liu, Y.-S. Kim, W.-H. Yeo, J.S. Park, J. Song, Y. Li, Y. Huang, A.M. Gorbach, J. A. Rogers, Ultrathin conformal devices for precise and continuous thermal characterization of human skin, Nat. Mater. 12 (10) (2013) 938–944, https://doi.org/10.1038/nmat3755.
[26] M. Ahmed, M.M. Chitteboyina, D.P. Butler, Z. Celik-Butler, Temperature sensor in a flexible substrate, IEEE Sens. J. 12 (5) (2012) 864–869, https://doi.org/10.1109/JSEN.2011.2166064.
[27] Y. He, Q. Gui, S. Liao, H. Jia, Y. Wang, Coiled fiber-shaped stretchable thermal sensors for wearable electronics, Adv. Mater. Technol. 1 (8) (2016) 1600170, https://doi.org/10.1002/admt.v1.810.1002/admt.201600170.
[28] S. Harada, K. Kanao, Y. Yamamoto, T. Arie, S. Akita, K. Takei, Fully printed flexible fingerprint-like three-axis tactile and slip force and temperature sensors for artificial skin, ACS Nano 8 (12) (2014) 12851–12857, https://doi.org/10.1021/nn506293y.
[29] K. Kanao, S. Harada, Y. Yamamoto, W. Honda, T. Arie, S. Akita, K. Takei, Highly selective flexible tactile strain and temperature sensors against substrate bending for an artificial skin, RSC Adv. 5 (38) (2015) 30170–30174, https://doi.org/10.1039/C5RA03110A.
[30] W. Shih, L. Tsao, C. Lee, M. Cheng, C. Chang, Y. Yang, K. Fan, Flexible temperature sensor array based on a graphite-polydimethylsiloxane composite, Sensors 10 (2010) 3597–3610, https://doi.org/10.3390/s100403597.
[31] X. Ren, K.e. Pei, B. Peng, Z. Zhang, Z. Wang, X. Wang, P.K.L. Chan, A low-operating-power and flexible active-matrix organic-transistor temperature-sensor array, Adv. Mater. 28 (24) (2016) 4832–4838, https://doi.org/10.1002/adma.v28.2410.1002/adma.201600040.
[32] B. Zhu, H. Wang, W.R. Leow, Y. Cai, X.J. Loh, M.-Y. Han, X. Chen, Silk fibroin for flexible electronic devices, Adv. Mater. 28 (22) (2016) 4250–4265, https://doi.org/10.1002/adma.v28.2210.1002/adma.201504276.
[33] S.-W. Hwang, H. Tao, D.-H. Kim, H. Cheng, J.-K. Song, E. Rill, M.A. Brenckle, B. Panilaitis, S.M. Won, Y.-S. Kim, Y.M. Song, K.J. Yu, A. Ameen, R. Li, Y. Su, M. Yang, D.L. Kaplan, M.R. Zakin, M.J. Slepian, Y. Huang, F.G. Omenetto, J. A. Rogers, A physically transient form of silicon electronics, Science 337 (6102) (2012) 1640–1644, https://doi.org/10.1126/science:1226325.
[34] M.S. Mannoor, H. Tao, J.D. Clayton, A. Sengupta, D.L. Kaplan, R.R. Naik, N. Verma, F.G. Omenetto, M.C. McAlpine, Graphene-based wireless bacteria detection on tooth enamel, Nat. Commun. 3 (2012) 763, https://doi.org/10.1038/ncomms1767.
[35] J. You, M. Li, B. Ding, X. Wu, C. Li, Crab chitin-based 2D soft nanomaterials for fully biobased electric devices, Adv. Mater. 29 (19) (2017) 1606895, https://doi.org/10.1002/adma.v29.1910.1002/adma.201606895.
[36] Z. Lv, J. Liu, X. Yang, D. Fan, J. Cao, Y. Luo, X. Zhang, Naturally derived wearable strain sensors with enhanced mechanical properties and high sensitivity, ACS Appl. Mater. Inter. 12 (19) (2020) 22163–22169, https://doi.org/10.1021/acsami.0c0434110.1021/acsami.0c04341.s001.
[37] I. Hussain, X. Ma, Y. Luo, Z. Luo, Fabrication and characterization of glycogen-based elastic, self-healable, and conductive hydrogels as a wearable strain-sensor for flexible e-skin, Polymer 210 (2020) 122961, https://doi.org/10.1016/j.polymer.2020.122961.
[38] K. Luo, Y. Yang, Z. Shao, Physically crosslinked biocompatible silk-fibroin-based hydrogels with high mechanical performance, Adv. Funct. Mater. 26 (6) (2016) 872–880, https://doi.org/10.1002/adfm.v26.610.1002/adfm.201503450.
[39] Y. Wang, J. Guo, L. Zhou, C. Ye, F.G. Omenetto, D.L. Kaplan, S. Ling, Design, fabrication, and function of Silk-Based nanomaterials, Adv. Funct. Mater. 28 (52) (2018) 1805305, https://doi.org/10.1002/adfm.v28.5210.1002/adfm.201805305.
[40] S. Ling, D.L. Kaplan, M.J. Buehler, Nanofibrils in nature and materials engineering, Nat. Rev. Mater. 3 (2018) 18016, https://doi.org/10.1038/natrevmats.2018.16.
[41] S. Ling, W. Chen, Y. Fan, K. Zheng, K. Jin, H. Yu, M.J. Buehler, D.L. Kaplan, Biopolymer nanofibrils: structure, modeling, preparation, and applications, Prog. Polym. Sci. 85 (2018) 1–56, https://doi.org/10.1016/j.progpolymsci.2018.06.004.
[42] C. Wang, K. Xia, Y. Zhang, D.L. Kaplan, Silk-based advanced materials for soft electronics, Accounts Chem. Res. 52 (10) (2019) 2916–2927, https://doi.org/10.1021/acs.accounts.9b00333.
[43] J. Liu, Q. Chen, Q. Liu, B. Zhao, S. Ling, J. Yao, Z. Shao, X. Chen, Intelligent silk fibroin ionotronic skin for temperature sensing, Adv. Mater. Technol 5 (7) (2020) 2000430, https://doi.org/10.1002/admt.v5.710.1002/admt.202000430.
[44] J. Liu, T. He, G. Fang, R. Wang, E.A. Kamoun, J. Yao, Z. Shao, X. Chen, Environmentally responsive composite films fabricated using silk nanofibrils and silver nanowires, J. Mater. Chem. C 6 (47) (2018) 12940–12947, https://doi.org/10.1039/C8TC04549F.
[45] Q. Wang, S. Ling, X. Liang, H. Wang, H. Lu, Y. Zhang, Self-healable multifunctional electronic tattoos based on silk and graphene, Adv. Funct. Mater. 29 (16) (2019) 1808695, https://doi.org/10.1002/adfm.v29.1610.1002/adfm.201808695.
[46] Z. Li, Z. Zheng, Y. Yang, G. Fang, J. Yao, Z. Shao, X. Chen, Robust protein hydrogels from silkworm silk, ACS Sustain. Chem. Eng. 4 (3) (2016) 1500–1506, https://doi.org/10.1021/acssuschemeng.5b0146310.1021/acssuschemeng.5b01463.s001.
[47] J.-W. Seo, H. Kim, KyuHan Kim, S.Q. Choi, H.J. Lee, Calcium-modified silk as a biocompatible and strong adhesive for epidermal electronics, Adv. Funct. Mater. 28 (36) (2018) 1800802, https://doi.org/10.1002/adfm.v28.3610.1002/adfm.201800802.
[48] X. Wu, J. Hou, M. Li, J. Wang, D.L. Kaplan, S. Lu, Sodium dodecyl sulfate-induced rapid gelation of silk fibroin, Acta Biomater. 8 (6) (2012) 2185–2192, https://doi.org/10.1016/j.actbio.2012.03.007.
[49] G.Y. Bae, S.W. Pak, D. Kim, G. Lee, D.H. Kim, Y. Chung, K. Cho, Linearly and highly pressure-sensitive electronic skin based on a bioinspired hierarchical structural array, Adv. Mater. 28 (26) (2016) 5300–5306, https://doi.org/10.1002/adma.201600408.
[50] M. Jung, S.K. Vishwanath, J. Kim, D.-K. Ko, M.-J. Park, S.-C. Lim, S. Jeon, Transparent and flexible mayan-pyramid-based pressure sensor using facile-transferred indium tin oxide for bimodal sensor applications, Sci. Rep. 9 (1) (2019), https://doi.org/10.1038/s41598-019-50247-4.
[51] A.K. Katz, J.P. Glusker, S.A. Beebe, C.W. Bock, Calcium ion coordination: a comparison with that of beryllium, magnesium, and zinc, J. Am. Chem. Soc. 118 (1996) 5752–5763, https://doi.org/10.1021/ja953943i.
[52] T. Kim, T. Lee, G. Lee, Y. Choi, S. Kim, D. Kang, M. Choi, Polyimide encapsulation of spider-inspired crack-based sensors for durability improvement, Applied Sciences 8 (2018) 367, https://doi.org/10.3390/app8030367.
[53] Y. Liu, Y. Hu, J. Zhao, G. Wu, X. Tao, W. Chen, Self-powered piezoionic strain sensor toward the monitoring of human activities, Small 12 (36) (2016) 5074–5080, https://doi.org/10.1002/smll.201600553.
[54] L. Zhou, X. Chen, Z. Shao, Y. Huang, D.P. Knight, Effect of metallic ions on silk formation in the mulberry silkworm, *bombyx mori*, J. Phys. Chem. B 109 (35) (2005) 16937–16945, https://doi.org/10.1021/jp050883m.
[55] S. Ling, Q. Zhang, D.L. Kaplan, F. Omenetto, M.J. Buehler, Z. Qin, Printing of stretchable silk membranes for strain measurements, Lab Chip 16 (13) (2016) 2459–2466, https://doi.org/10.1039/C6LC00519E.
[56] M.R. Conde, Properties of aqueous solutions of lithium and calcium chlorides: Formulations for use in air conditioning equipment design, Int. J. Therm. Sci. 43 (4) (2004) 367–382, https://doi.org/10.1016/j.ijthermalsci.2003.09.003.
[57] X.P. Morelle, W.R. Illeperuma, K. Tian, R. Bai, Z. Suo, J.J. Vlassak, Highly stretchable and tough hydrogels below water freezing temperature, Adv. Mater. 30 (35) (2018) 1801541, https://doi.org/10.1002/adma.v30.3510.1002/adma.201801541.
[58] T. Someya, Y. Kato, T. Sekitani, S. Iba, Y. Noguchi, Y. Murase, H. Kawaguchi, T. Sakurai, Conformable, flexible, large-area networks of pressure and thermal sensors with organic transistor active matrixes, Proc. Natl. Acad. Sci. U. S. A. 102 (35) (2005) 12321–12325, https://doi.org/10.1073/pnas.0502392102.
[59] T. Yokota, Y. Inoue, Y. Terakawa, J. Reeder, M. Kaltenbrunner, T. Ware, K. Yang, K. Mabuchi, T. Murakawa, M. Sekino, W. Voit, T. Sekitani, T. Someya, Ultraflexible, large-area, physiological temperature sensors for multipoint measurements, Proc. Natl. Acad. Sci. U. S. A. 112 (47) (2015) 14533–14538, https://doi.org/10.1073/pnas.1515650112.
[60] J. Jeon, H.-B.-R. Lee, Z. Bao, Flexible wireless temperature sensors based on Ni microparticle-filled binary polymer composites, Adv. Mater. 25 (6) (2013) 850–855, https://doi.org/10.1002/adma.v25.610.1002/adma.201204082.
[61] T.Q. Trung, S. Ramasundaram, S.W. Hong, N.-E. Lee, Flexible and transparent nanocomposite of reduced graphene oxide and P(VDF-TrFE) copolymer for high thermal responsivity in a field-effect transistor, Adv. Funct. Mater. 24 (22) (2014) 3438–3445, https://doi.org/10.1002/adfm.201304224.
[62] G. Chen, N. Matsuhisa, Z. Liu, D. Qi, P. Cai, Y. Jiang, C. Wan, Y. Cui, W.R. Leow, Z. Liu, S. Gong, K.-Q. Zhang, Y. Cheng, X. Chen, Plasticizing silk protein for on-skin stretchable electrodes, Adv. Mater. 30 (21) (2018) 1800129, https://doi.org/10.1002/adma.v30.2110.1002/adma.201800129.
[63] T. NAGAI, Y. TABARA, M. IGASE, J. NAKURA, T. MIKI, K. KOHARA, Migraine is associated with enhanced arterial stiffness, Hypertens. Res. 30 (7) (2007) 577–583, https://doi.org/10.1291/hypres.30.577.
[64] W. Nichols, Clinical measurement of arterial stiffness obtained from noninvasive pressure waveforms, Am. J. Hypertens. 18 (2005) 3–10, https://doi.org/10.1016/j.amjhyper.2004.10.009.
[65] C. Pang, G.-Y. Lee, T.-i. Kim, S.M. Kim, H.N. Kim, S.-H. Ahn, K.-Y. Suh, A flexible and highly sensitive strain-gauge sensor using reversible interlocking of nanofibres, Nat. Mater. 11 (9) (2012) 795–801, https://doi.org/10.1038/nmat3380.
[66] D. Kim, T. Quang Trung, B. Hwang, J. Kim, S. Jeon, J. Bae, J. Park, N. Lee, A sensor array using multi-functional field-effect transistors with ultrahigh sensitivity and precision for bio-monitoring, Sci. Rep. 5 (1) (2015), https://doi.org/10.1038/srep12705.
[67] S. Munir, B. Jiang, A. Guilcher, S. Brett, S. Redwood, M. Marber, P. Chowienczyk, Exercise reduces arterial pressure augmentation through vasodilation of muscular arteries in humans, Am. J. Physiol.-Heart Circul. Physiol. 294 (4) (2008) H1645–H1650, https://doi.org/10.1152/ajpheart.01171.2007.
[68] C. Wang, X. Li, E. Gao, M. Jian, K. Xia, Q.i. Wang, Z. Xu, T. Ren, Y. Zhang, Carbonized silk fabric for ultrastretchable, highly sensitive, and wearable strain sensors, Adv. Mater. 28 (31) (2016) 6640–6648, https://doi.org/10.1002/adma.201601572.